# Phase Transitions in Aqueous $NH_4HSO_4$ Solutions

**Thomas Koop,† Allan K. Bertram, Luisa T. Molina, and Mario J. Molina***

*Department of Earth, Atmospheric and Planetary Sciences and of Chemistry, Massachusetts Institute of Technology, Cambridge, Massachusetts 02139*

*Received: June 21, 1999; In Final Form: September 21, 1999*

Differential scanning calorimetry has been employed to investigate phase transitions in aqueous $NH_4HSO_4$ solutions 0 to 60 wt %. Bulk samples, 3 $\mu$L in volume, have been used to determine the $NH_4HSO_4$ phase diagram down to 195 K. The results are in very good agreement with the ice, letovicite, and sulfuric acid tetrahydrate melting points predicted by the thermodynamic model of Clegg et al. (*J. Phys. Chem. A* **1998**, *102*, 2137−2154). In addition, emulsified samples have been employed to investigate the kinetics of ice nucleation in micrometer-sized aqueous $NH_4HSO_4$ droplets. The observed ice freezing points range from 234 K for 0 wt % to 179 K for 35 wt %. A thermodynamic model has been used to apply these freezing point data to the formation of cirrus clouds. The results indicate that the homogeneous nucleation of ice particles in cirrus clouds requires saturation ratios with respect to ice ranging from about 1.5 at 230 K to about 1.7 at 200 K.

## 1. Introduction

Cirrus clouds cover up to about 20−30% of the earth and thus play an important role in the earth's atmosphere.[1] These clouds strongly affect the radiative properties of the earth by scattering incoming sunlight and absorbing long-wavelength radiation from the earth's surface. The optical properties of cirrus clouds depend on their formation conditions, which are mainly controlled by preexisting aerosols. However, the exact role aerosols play in the formation of cirrus clouds is still poorly understood and is one of the main uncertainties in assessing the global radiation budget.[2,3] In addition, an assessment of the effect of aircraft and contrails on the cloud coverage of the upper troposphere requires a detailed microphysical understanding of the formation of cirrus clouds.[3,4]

Up to now it has been generally believed that aerosols in the upper troposphere consist mainly of aqueous $H_2SO_4$.[5] However, recent measurements during the SUCCESS field campaign have shown that considerable and highly variable amounts of ammonia (as $NH_4^+$) and nitric acid (as $NO_3^-$) can be present in upper tropospheric aerosols over the continental United States.[6] Also, theoretical studies have pointed out the importance of ammoniated sulfate aerosols for cirrus cloud formation.[7,8] These studies suggest that cirrus clouds can form from a variety of multicomponent aerosols. Only a few experimental studies, however, have investigated the kinetics of ice formation from relevant aerosols, i.e., from $H_2SO_4/H_2O$,[9,10] $HNO_3/H_2O$ and $HNO_3/H_2SO_4/H_2O$,[11] and $(NH_4)_2SO_4$.[12]

In this paper we focus on the thermodynamics and the phase-transition kinetics of aqueous $NH_4HSO_4$ solutions, i.e., partially neutralized sulfate aerosols. There are only limited data on the $NH_4HSO_4/H_2O$ system at low temperatures. Imre et al.[13] were the first to report a phase diagram using an electrodynamic balance aerosol experiment. Their data are in disagreement with results from a thermodynamic model of the $NH_3/H_2SO_4/H_2O$ system developed by Clegg et al.[14] In contrast, very recent bulk measurements down to 246 K show very good agreement with results from the model.[15,16]

In addition, we present new data on the $NH_4HSO_4/H_2O$ phase diagram including phase-transition temperatures down to 195 K and also on the nucleation of ice from $NH_4HSO_4/H_2O$ droplets. The implications for cirrus cloud formation are also discussed.

## 2. Experimental Section

**2.1. General Description.** Differential scanning calorimetry (DSC) is a standard technique for characterizing phase transitions in condensed-phase samples. The experimental setup employed in this paper has been described in detail previously.[11]

The DSC technique consists of warming or cooling a sample cell and a reference cell at a predetermined rate, while the temperature difference between the two cells is always maintained close to zero by heating with individual electric heaters. What is monitored is the difference between the electric power supplied to heat the sample cell and the reference cell. If a sample releases latent heat during freezing, less power is required to heat the sample cell, and thus, a signal can be observed (see Figure 1).

In this study we used a Perkin-Elmer DSC-7 with a low-temperature head and a glovebox addition. The glovebox was purged with dry air, and the sample and reference cell compartments were purged with helium gas to prevent any unwanted water condensation. The operational temperature of our instrument ranged from 100 to 450 K, and only a few milligrams of sample were required for each measurement. A scanning rate of 5 K $min^{-1}$ during heating and cooling was chosen for both bulk and emulsion sample measurements. This rate yields the best sensitivity while maintaining a high degree of accuracy.[11]

Solutions of $(NH_4)HSO_4$ were prepared by adding deionized water to $(NH_4)HSO_4$ crystals (EM Science, ≥99.8%). We ensured the crystals were water-free by evaporating a prepared solution and determining the mass before and after evaporation.

* To whom correspondence should be addressed.
† Current address: Swiss Federal Institute of Technology, Atmospheric Physics, Hoenggerberg HPP, 8093 Zurich, Switzerland.

10.1021/jp992033a CCC: $18.00 
Published on Web 10/22/1999

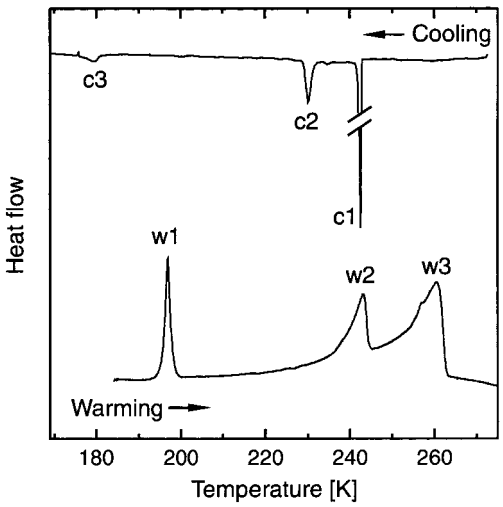


**Figure 1.** DSC bulk experiment with 3 $\mu$L of a 26.6 wt % $NH_4HSO_4$ solution: (top trace) cooling experiment; (bottom trace) warming experiment. The labels c1−c3 indicate freezing peaks, and labels w1−w3 denote melting peaks. The freezing peak labeled c1 was split to reduce its size, allowing c2 and c3 to be easily observed.

**2.2. Bulk Samples.** The cells used in the bulk experiments consisted of a stainless steel ferrule placed in a stainless steel cup. The ferrule had an inner diameter of $^1/_{16}$ in. and a height of 1.5 mm, yielding a total sample volume of about 3 $\mu$L. To avoid evaporation of water from the sample during an experiment, the ferrule was covered with a thin glass plate approximately 170 $\mu$m in thickness. The sealing between the cup, the ferrule, and the glass cover was achieved by a thin layer of Halocarbon grease. The cell temperature was calibrated using a Perkin-Elmer two-point calibration program with pure water (deionized, melting point of 273.15 K) and cyclohexane (EM Science, solid−solid transition at 186.09 K) as the standards. This calibration was used for both cooling and heating experiments. Before each experimental run the sample cell was completely filled with approximately 3 $\mu$L of one of the $NH_4HSO_4$ solutions described above and placed into the DSC, and then the sample was cooled to 153 K at a rate of 5 K $min^{-1}$. Subsequently, it was heated to 283 K at a rate of 5 K $min^{-1}$.

A typical experiment is depicted in Figure 1, which shows the cooling and heating of a sample of $NH_4HSO_4$, 26.6 wt % in composition. Three freezing signals are clearly visible in the cooling run corresponding to the nucleation and freezing of ice (c1), letovicite (c2), and sulfuric acid tetrahydrate (SAT, c3), where letovicite is solid $(NH_4)_3H(SO_4)_2$. When the sample is warmed, three peaks are visible corresponding to different melting points (w1, ice/letovicite/SAT eutectic; w2, the point at which the last letovicite melts in equilibrium with ice and liquid; w3, the melting point of ice). From the peaks w1 to w3 the phase diagram of the $NH_4HSO_4/H_2O$ system can be constructed (see below).

**2.3. Emulsion Samples.** The emulsion samples were prepared by mixing 0.4 mL of an aqueous solution with 2.5 mL of an oil phase containing approximately 80 wt % halocarbon oil series 0.8 (Halocarbon Products Corporation) and 20 wt % lanolin (Aldrich Chemical). Emulsification was achieved by shaking the aqueous solution−oil mixture at room temperature manually for about 15 s and then with a high speed mixer at a frequency of 1400 Hz for 2 min. For each experiment approximately 22 $\mu$L of the emulsion was placed in a disposable aluminum sample pan. All samples were prepared just before the experiment to minimize degradation of the emulsion due to slow chemical reactions. The procedure and the properties of emulsified aqueous solutions have been described in detail in our previous publication.[11] Calibration of the cell temperature for the emulsified samples was performed by using pure water (deionized, melting point at 273.15 K) and a 41 wt % solution of absolute methanol in water (eutectic melting point of ice and methanol monohydrate, $CH_3OH{\cdot}H_2O$, at 168.65 K[17]). As in the bulk experiments, cooling and heating rates of 5 K $min^{-1}$ were used in all emulsion experiments. The DSC signal during freezing and melting in an emulsion sample is basically identical to the one in bulk samples and emulsion DSC runs looked comparable to Figure 1.

One of the advantages of studying phase transitions using emulsions is that the aqueous droplets are isolated by the oil phase, and hence, their composition is fixed. In addition, each freezing point determination has a statistical significance, since a large number of droplets ($\geq 10^6$) is monitored. The emulsification procedure results in droplets of about 1−10 $\mu$m in size as determined by optical microscopy. The corresponding uncertainty in the freezing point is small (see section 3.2.2. below).

The extent of crystallization of the total droplet distribution corresponds to the mass fraction of the crystallized phase and can be determined by integrating the exothermic crystallization peak in a DSC emulsion experiment. The freezing points of the emulsified droplets were defined as the temperature at which 90% of the aqueous sample mass was frozen.

**2.4. Optical Microscopy.** In a third type of experiment we studied the freezing of highly concentrated droplets using an optical microscopy technique developed in our laboratory.[10] The experimental setup is identical to the one used in our earlier work.[10] Briefly, aerosols were deposited on a hydrophobic quartz crucible that was placed onto the cooling stage of an optical microscope. The phase, liquid or crystalline, was determined from the optical appearance of the particles.

## 3. Results and Discussion

**3.1. $NH_4HSO_4$ Phase Diagram.** The results obtained during the warming cycles of the bulk measurements are shown in Figure 2a and Table 1. Each point in Figure 2a represents the average phase-transition temperature of at least three runs at a given composition. The error bars indicate the standard deviation of the individual runs from the mean plus an estimated uncertainty of 0.5 K in the absolute accuracy of the temperature after calibration. Also shown as lines are the equilibrium conditions of ice and liquid (dotted), letovicite and liquid (dashed), ice, letovicite and liquid (solid), and finally ice, letovicite, SAT, and liquid (dash−dotted) as calculated from the thermodynamic model of Clegg et al.[14] The measured phase-transition temperatures are in excellent agreement with the model calculations for these crystalline phases at temperatures above 220 K and have only a slight deviation of about 1 K for the transitions at 196 K. This agreement suggests that indeed ice, letovicite, and SAT are formed in our experiments. In the following we will support this conclusion and also compare our results to other measurements reported on the aqueous $NH_4HSO_4$ system.

Recently, Yao et al.[15] and Chelf and Martin[16] performed melting point measurements of aqueous $NH_4HSO_4$ solutions using bulk samples with volumes of 40 and 100 mL at temperatures greater than 246 K. The melting points determined in both of these studies agree closely with the model of Clegg et al.[14] In addition, Chelf and Martin[16] also analyzed the composition of the liquid in equilibrium with the precipitates and found that letovicite was the crystalline solid that had the highest melting point at concentrations greater than 47 wt %

**TABLE 1: Melting Points of $NH_4HSO_4$ Solutions**[a]

| conc [wt %] | $T_1$(exp) [K] | $T_1$(mod) [K] | $T_2$(exp) [K] | $T_2$(mod) [K] | $T_3$(exp) [K] | $T_3$(mod) [K] |
|---|---|---|---|---|---|---|
| 5.3 | 195.3 ± 1.3 | 197.0[b] | 243.5 ± 0.7 | 242.9[c] | 271.2 ± 0.6 | 271.4[f] |
| 10.7 | 195.6 ± 0.8 | 197.0[b] | 243.3 ± 0.7 | 242.9[c] | 269.7 ± 0.8 | 269.6[f] |
| 15.8 | 195.7 ± 0.8 | 197.0[b] | 243.0 ± 0.8 | 242.9[c] | 267.3 ± 0.8 | 267.5[f] |
| 21.2 | 195.9 ± 0.7 | 197.0[b] | 243.1 ± 0.7 | 242.9[c] | 264.5 ± 0.7 | 264.8[f] |
| 26.6 | 195.7 ± 0.6 | 197.0[b] | 242.7 ± 0.7 | 242.9[c] | 260.4 ± 1.0 | 261.1[f] |
| 30.1 | 196.2 ± 0.7 | 197.0[b] | 243.1 ± 0.7 | 242.9[c] | 257.0 ± 1.2 | 258.1[f] |
| 34.7 | 196.1 ± 0.7 | 197.0[b] | 243.0 ± 0.7 | 242.9[c] | 253.1 ± 0.9 | 253.2[f] |
| 39.5 | 195.9 ± 0.7 | 197.0[b] | 242.8 ± 0.6 | 242.9[c] | 246.3 ± 0.9 | 246.8[f] |
| 44.2 | 195.8 ± 0.7 | 197.0[b] | 241.7 ± 0.8 | 241.9[d] | 248.7 ± 1.2 | 248.2[g] |
| 49.9 | 196.2 ± 0.7 | 197.0[b] | 238.7 ± 0.7 | 238.6[d] | *e* | 261.1[g] |
| 54.4 | 196.2 ± 0.9 | 197.0[b] | 234.5 ± 1.0 | 234.5[d] | *e* | 270.4[g] |
| 59.6 | 196.0 ± 0.7 | 197.0[b] | 225.8 ± 0.8 | 227.0[d] | *e* | 280.3[g] |

[a] conc is the overall $NH_4HSO_4$ concentration of the sample [in wt %], $T_i$(exp) are the experimentally determined phase-transition temperatures and their standard deviations [in K] (see data points in Figure 2a), and $T_i$(mod) are certain phase-transition temperatures [in K] as calculated from the model of Clegg et al.[14] (see lines in Figure 2a). [b] Ternary ice/letovicite/SAT eutectic temperature. [c] Ice melting point in equilibrium with letovicite. [d] Letovicite melting point in equilibrium with ice. [e] Melting points could not be determined because of sensitivity problems. [f] Ice melting point. [g] Letovicite melting point.

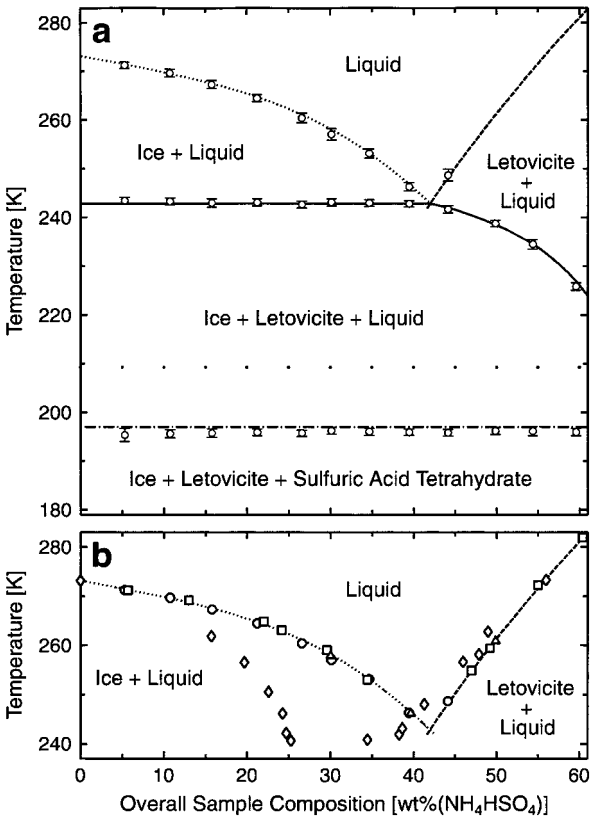


**Figure 2.** (a) $NH_4HSO_4/H_2O$ phase diagram from 0 to 60 wt %. Each circle indicates the average phase-transition temperature as experimentally observed with DSC bulk samples. Also shown as thick lines are the equilibrium lines of ice with liquid (dotted), letovicite with liquid (dashed), ice and letovicite with liquid (solid), and finally ice, letovicite, and SAT with liquid (dash−dotted) as calculated from the thermodynamic model of Clegg et al.[14] The labels indicate which mixture of phases is stable at certain temperatures and compositions. The lightly dotted horizontal line at about 209 K indicates the calculated ternary eutectic of ice, letovicite, and SAH. (b) Comparison of various melting point measurements in the literature. The open circles and lines are as in panel a. The triangles and squares represent the bulk-phase measurements by Yao et al.[15] and Chelf and Martin,[16] respectively. The diamonds indicate the single aerosol data by Imre et al.[13]

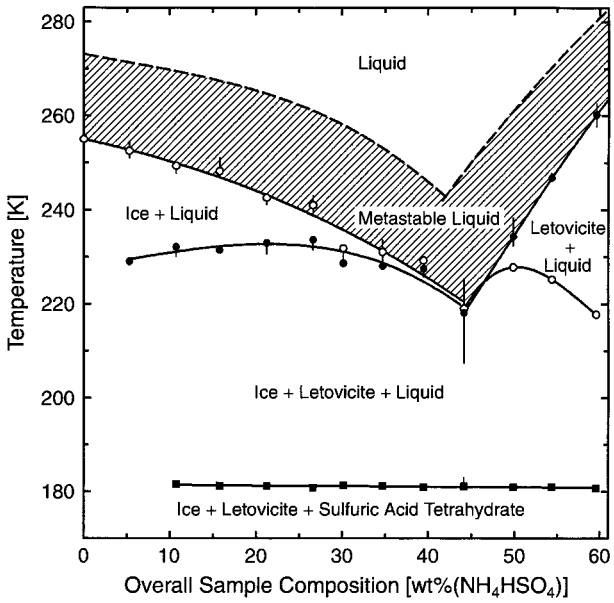


**Figure 3.** Freezing points of $NH_4HSO_4$ bulk samples 3 $\mu$L in volume measured with a cooling rate of 5 K $min^{-1}$. Each point represents the median of several experiments, and the solid lines are fits to the data points. Open circles represent freezing of ice; solid circles represent freezing of letovicite; squares represent freezing of SAT. The dashed lines indicate the melting point curves of ice and letovicite. The labels indicate regions of stability of the different phase mixtures. In the shaded region, $NH_4HSO_4$ aerosols in the atmosphere do not freeze homogeneously but exist as metastable liquid droplets.

$NH_4HSO_4$. Letovicite ($(NH_4)_3H(SO_4)_2$) is more alkaline than $NH_4HSO_4$; that is, it contains a larger $NH_3/H_2SO_4$ ratio (3:2) than $NH_4HSO_4$ (1:1). Hence, if letovicite were formed from $NH_4HSO_4$ solution, the remaining liquid would become more acidic; i.e., it would contain relatively more $H_2SO_4$ (an analytical expression can be found in ref 16). This implies that a complete solidification of a $NH_4HSO_4$ solution requires the formation of a third crystalline phase apart from ice and letovicite. This is what we observed in our experiments; i.e., all solutions investigated in this study exhibited three phase transitions. Unfortunately we could not detect the exact melting points for letovicite at concentrations larger than 44.2 wt % with a satisfactory accuracy, but we did observe three phase transitions upon cooling in these experiment as well (see Figure 3). Note that when letovicite forms, the remaining liquid assumes a ratio of $NH_3/H_2SO_4$ smaller than 1:1, and hence, the letovicite/liquid curve (dashed line in Figure 2) and the ice/letovicite/liquid curve (solid line) should not be used to deduce the composition of the remaining liquid.

The dotted horizontal line at 209 K in Figure 2a indicates the ternary ice/letovicite/SAH eutectic, which according to the Clegg et al. model is the highest ternary eutectic in the $NH_3/$

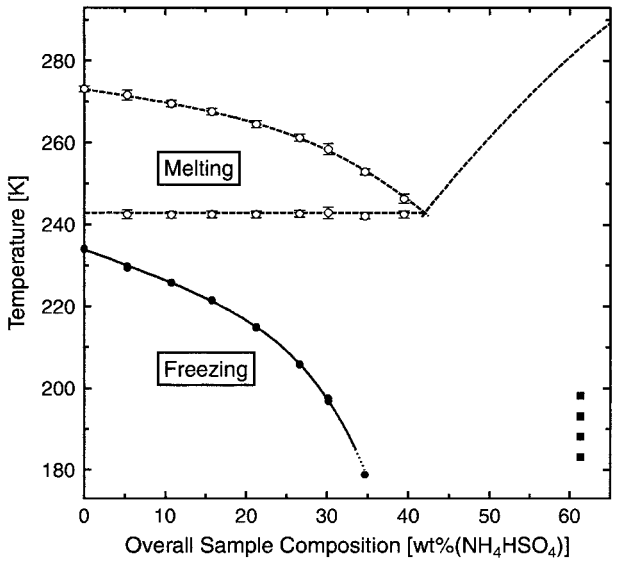


**Figure 4.** Experimentally observed melting points (open circles) and ice freezing points (solid circles) of emulsified aqueous $NH_4HSO_4$ droplets. The solid line is a fit to the freezing data, while the dotted line is an extension for which the parameters given in Tables 2 and 3 are outside their validity range. The dashed lines indicate the ice melting point curve, the letovicite melting point curve, and the ice/letovicite/liquid coexistence temperature as calculated with the model of Clegg et al.[14] (see Figure 2). The squares in the lower right corner indicate the conditions under which letovicite nucleation experiments were performed (see text).

$H_2SO_4/H_2O$ system when ice and letovicite are present. Our experiments indicate that SAT formed although SAH (sulfuric acid hemihexahydrate) was already supersaturated at higher temperatures and SAH had a higher supersaturation than SAT at any temperature below 209 K. The same behavior has been observed in the ternary $HNO_3/H_2SO_4/H_2O$ system where ice, nitric acid trihydrate (NAT), and SAT often formed, although the combination of ice, NAT, and SAH was the stable ternary eutectic.[18−20] A likely explanation for this observation is that the compatibility between ice and SAT is higher than between ice and SAH; thus, once ice is present, SAT nucleates more readily than SAH. The temperature for the ice/letovicite/SAT eutectic observed in our experiments is 195.9 K compared to 197.0 K predicted by the Clegg et al. model. This deviation is small given the fact that large extrapolations to low temperatures were required in the model, since only high-temperature data ($\geq$273 K) were available.

Figure 2b shows a comparison of various melting point studies for the $NH_4HSO_4$ system. Our data agree closely with the measurements by Yao et al.[15] and Chelf and Martin.[16] However, our measurements do not agree with the experimental results obtained by Imre et al.[13] The largest deviations occur at the ice melting point curve with differences in temperature of up to 20 K at about 26 wt % $NH_4HSO_4$. This deviation cannot be explained by the fact that we used bulk samples while Imre et al.[13] employed a single aerosol experiment. The melting of ice is not a kinetically driven phase transition but occurs at the equilibrium value. Hence, no size dependence of the ice melting point curve is expected for droplets in the micrometer range. This is supported by our emulsion experiments reported below (see Figure 4), which show the same melting temperatures as the bulk samples shown in Figure 2.

In addition, Imre et al.[13] report that $NH_4HSO_4$ and $NH_4HSO_4 \cdot 8H_2O$ formed in their aerosol experiment rather than letovicite or SAT. We can exclude the formation of $NH_4HSO_4 \cdot 8H_2O$ in our experiments for the following reasons. If $NH_4HSO_4 \cdot 8H_2O$ were formed, one would expect the latent heat released at the ice/$NH_4HSO_4 \cdot 8H_2O$ eutectic to show a maximum at the eutectic composition, which is reported to be at about 26 wt % $NH_4HSO_4$ by Imre et al.[13] (see note 21). In contrast, both phase transitions at ~243 and ~196 K in our experiments show a monotonic increase in latent heat release for concentrations up to 44.2 and 59.6 wt %, respectively. These observations are in agreement with the formation of ice, letovicite, and SAT.

It is interesting to note that the $NH_4HSO_4$ melting point curve reported by Imre et al.[13] agrees closely with the letovicite melting point curve in the bulk experiments and the model. Also, Imre et al.[13] reported the $NH_4HSO_4/NH_4HSO_4 \cdot 8H_2O$ peritectic to be at 243.2 K, which closely agrees with the ice/letovicite/liquid coexistence temperature at a concentration smaller than approximately 43 wt % $NH_4HSO_4$ measured in this paper (243.1 K) and calculated by the Clegg et al. model (242.9 K). Whether these agreements are coincidences or do have a physical or experimental meaning remains to be determined. At present the reason for the discrepancies between the phase diagram of Imre et al.[13] and our phase diagram is unclear; however, considering the good agreement between our studies and the experimental studies by Yao et al.[15] and Chelf and Martin,[16] we believe our phase diagram is correct. The very good agreement between the last three studies and the model by Clegg et al.[14] suggests that this model is applicable at upper tropospheric temperatures.

**3.2. Supercooling Experiments.** *3.2.1. Bulk Experiments.* The formation of a crystalline phase from a liquid requires a nucleation process and thus usually exhibits a supercooling.[22] In addition, the nucleation probability is directly proportional to the volume of the liquid. Hence, bulk-phase supercooling studies can only provide an upper limit for the conditions (i.e., concentration and temperature) at which aerosols in the atmosphere will exhibit phase transitions.[20] This implies that an aerosol droplet will most likely crystallize at a significantly lower temperature than a bulk sample of the same composition. Here, we present bulk supercooling studies in order to get a first estimate of the freezing behavior of the $NH_4HSO_4$ system. Figure 3 shows the freezing point measurements performed with bulk samples of 3 $\mu$L volume. Each point indicates the median freezing temperature of three or more samples at each concentration. The open circles indicate the freezing of ice, the solid circles the freezing of letovicite, and the squares the freezing of SAT (see peaks c1−c3 in Figure 1 for comparison). The identities of the solid phases were determined by warming each sample and determining its melting point. For comparison the melting point curves for ice and letovicite are shown as dashed lines. All solutions exhibit a supercooling of about 20 K for both ice (below about 40 wt %) and letovicite (above about 40 wt %), which is about the same as that reported by Chelf and Martin[16] for 100 mL samples. Given the fact that the sample volumes used in these experiments are several orders of magnitude larger than the volume of atmospheric aerosols, the shaded area gives conditions at which the aerosols will not freeze homogeneously in the atmosphere. However, this area only provides an upper limit and the freezing temperatures of aerosol droplets of the same composition are most likely much lower. For example, water droplets in the micrometer size range freeze only at temperatures of about 234 K, ~20 K below the upper limits shown in Figure 3. Therefore, we have investigated emulsified droplets in the micrometer range to get a better estimate of the ice freezing ability of $NH_4HSO_4/H_2O$ aerosols in the atmosphere.

*3.2.2. Emulsion Experiments.* We have used the emulsion technique successfully for similar studies with aqueous $HNO_3/$

**TABLE 2: Critical Ice Nucleation Temperature as a Function of $NH_4HSO_4$ Concentration for Micrometer-Sized Aqueous $NH_4HSO_4$ Droplets[a]**

| | $A_0$ | $A_1$ | $A_2$ | $A_3$ | $A_4$ |
|---|---|---|---|---|---|
| $T^*$ | 233.84 | −0.711 | $-2.97 \times 10^{-3}$ | $-7.70 \times 10^{-6}$ | $-8.35 \times 10^{-9}$ |

[a] T* can be calculated from $T^* = A_0 + A_1\,\mathrm{wt} + A_2\,\mathrm{wt}^2 + A_3\,\mathrm{wt}^4 + A_4\,\mathrm{wt}^6$, where $T^*$ is the critical ice nucleation temperature [in K] and wt is the $NH_4HSO_4$ concentration [in wt %]. This relation is valid from 0 to 33.5 wt %.

$H_2O$ and $HNO_3/H_2SO_4/H_2O$ droplets.[11] The experimental results are shown in Figure 4. The solid circles show the measured ice freezing points. The solid line is a fit through the data, and the parameters for this curve are given in Table 2. For comparison the melting point curves of ice and letovicite as well as the ice/letovicite/liquid coexistence curve are also shown as dashed lines in Figure 4. No freezing of ice was observed for concentrations greater than 34.7 wt % $NH_4HSO_4$. We believe that the ice freezing points reported here are not influenced by heterogeneous processes at the aqueous phase/oil interface. Using the tabulated homogeneous nucleation rate coefficients for the nucleation of ice from pure water,[22] we calculate freezing temperatures (90% of the particles frozen) at a cooling rate of 5 K $min^{-1}$ of 233.3 K for 1 $\mu$m particles, 234.3 K for 2.5 $\mu$m particles, 234.9 K for 5 $\mu$m particles, and 235.6 K for 10 $\mu$m particles. First, this shows that the freezing points are rather insensitive ($\Delta T \approx 2.3$ K) to a variation in droplet size from 1 to 10 $\mu$m, which is the uncertainty in our experimental droplet size. Second, these values are in very good agreement with our measurements of emulsified water droplets that froze at 234.1 K, thus supporting our hypothesis that we are indeed monitoring homogeneous nucleation of ice. It also suggests that the freezing points reported here correspond to droplets of about 2−2.5 $\mu$m.

As an additional check for the composition of the aqueous droplets and the nature of the crystallized solid phases, all samples were heated afterward and the melting points were determined similarly as in the bulk-phase experiments. The emulsion melting points for concentrations up to 34.7 wt % $NH_4HSO_4$ are shown as open circles in Figure 4 and are in very good agreement with the bulk-phase results. We note that the ternary ice/letovicite/SAT eutectic measured in the emulsion system is about 2 K lower than in the bulk-phase system. However, the bulk experiments were specifically designed and optimized for the detection of melting points in terms of sensitivity and accuracy. Thus, we do believe the bulk-phase melting points to be more accurate.

*3.2.3. Microscope Experiments.* We did not observe letovicite freezing in emulsified droplets with concentrations between 39.5 and 59.6 wt % $NH_4HSO_4$ at temperatures greater than 180 K. Therefore, we used the optical microscopy technique developed in our laboratory[10] to study the freezing of letovicite from larger aqueous $NH_4HSO_4$ droplets. Twenty-one droplets with an average equivalent diameter of 34.4 $\mu$m were deposited on a hydrophobic quartz crucible and cooled to a fixed temperature. The particles were observed for about 60 min with an optical microscope, and the entire experiment was recorded on videotape. Subsequently, the particles were warmed to their melting point from which the particle composition was determined to be 61.4 wt % $NH_4HSO_4$. Experiments were performed at 198.2, 193.2, 188.2, and 183.2 K; the experimental conditions are indicated in Figure 4 by the solid squares in the lower right. The amount of time it took the individual droplets to nucleate at each temperature was noted, and the results are shown as the fraction of particles that remained liquid as a function of time in Figure 5. A clear temperature trend can be observed with

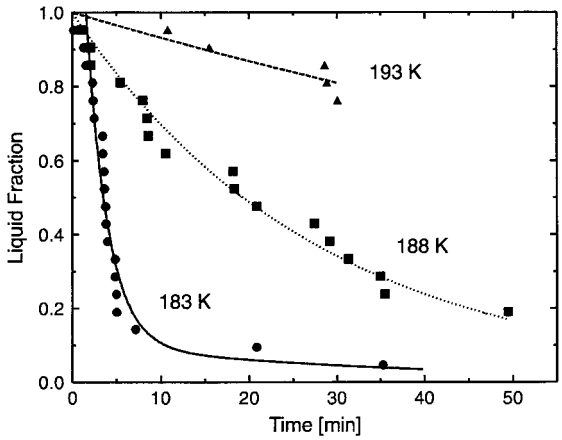


**Figure 5.** Fraction of 34.4 $\mu$m $NH_4HSO_4$ droplets 61.4 wt % in composition that remained liquid as a function of time for different temperatures. Each point corresponds to a nucleation event. The curves are exponential fits to the data as described in the text.

nucleation becoming faster at lower temperatures. At 198.2 K none of the droplets froze within an observation time of 30 min. Since nucleation is a stochastic process, the fraction of liquid droplets is expected to decrease exponentially with time.[20] Consequently, the experimental data were fitted to exponential functions; the resulting curves are shown in Figure 5. Both the 193.2 and 188.2 K data were fit to single exponentials. However, a sum of two weighted exponentials (see eq 19 in ref 20) was required to fit the 183.2 K data, which suggests two different processes are occurring at the lowest temperature. In addition, a constant term of ∼2 min was added to the double-exponential function because of the observed slow crystal growth at 183.2 K. We cannot give a conclusive explanation for the two different processes at 183.2 K, but we provide two suggestions. First, the faster process is due to heterogeneous nucleation and the slower one is due to homogeneous nucleation. Alternatively, the faster process is due to homogeneous nucleation while the slower one is due to mass transport from unfrozen particles to frozen particles (mass transport will cause the unfrozen particles to become slightly less concentrated). When the data are fit to a double exponential, the highest possible rate for the faster of the two processes is determined and hence is the most conservative estimate for an upper bound of the homogeneous nucleation rate coefficient. The upper confidence limits (99.9%) were calculated using Poisson statistics[20] and are $J_{hom}(183.2\ \mathrm{K}) = 7.5 \times 10^5\ \mathrm{cm}^{-3}\ \mathrm{s}^{-1}$, $J_{hom}(188.2\ \mathrm{K}) = 4.8 \times 10^4\ \mathrm{cm}^{-3}\ \mathrm{s}^{-1}$, $J_{hom}(193.2\ \mathrm{K}) = 1.2 \times 10^4\ \mathrm{cm}^{-3}\ \mathrm{s}^{-1}$, and $J_{hom}(198.2\ \mathrm{K}) = 8.6 \times 10^3\ \mathrm{cm}^{-3}\ \mathrm{s}^{-1}$, where $J_{hom}(T)$ refers to the homogeneous nucleation rate coefficient at temperature $T$. These values imply that it would take about 163 days to nucleate letovicite in 50% of 0.5 $\mu$m aerosols containing 61.4 wt % $NH_4HSO_4$ at 183.2 K. Hence, higher concentrations are required to freeze letovicite from $NH_4HSO_4$ aerosols on relevant atmospheric time scales.

## 4. Atmospheric Implications

Until recently, cirrus clouds were believed to form from sulfate aerosols, which are ubiquitous in the upper troposphere.[5] However, recent in situ measurements over the continental U.S. showed that significant amounts of $NH_3$ can be present in upper tropospheric aerosols.[6] Hence, it is important to understand how ice particles in cirrus clouds form from ammoniated aerosols.[7,8] In the following section we describe thermodynamic calculations we performed in order to relate the ice freezing results from emulsified aqueous $NH_4HSO_4$ droplets presented above to the atmosphere.

**TABLE 3: Critical Ice Nucleation Parameters, $X^*$, as a Function of the Water Vapor Pressure $P_{H_2O}$ for Micrometer-Sized Aqueous $NH_4HSO_4$ Droplets[a]**

| $X^*$ | $A_0$ | $A_1$ | $A_2$ | $A_3$ |
|---|---|---|---|---|
| $T^*$ | $2.4973 \times 10^{+2}$ | $1.065 \times 10^{+1}$ | $4.465 \times 10^{-1}$ | $1.178 \times 10^{-2}$ |
| $a_w^*$ | $1.0579 \times 10^{+0}$ | $3.633 \times 10^{-2}$ | $-3.050 \times 10^{-4}$ | $-1.390 \times 10^{-4}$ |
| $S_{ice}^*$ | $1.3176 \times 10^{+0}$ | $-1.056 \times 10^{-1}$ | $-9.180 \times 10^{-3}$ | $-3.130 \times 10^{-4}$ |
| $\Delta T^*$ | $-2.9668 \times 10^{+0}$ | $4.109 \times 10^{-1}$ | $7.679 \times 10^{-2}$ | $3.619 \times 10^{-3}$ |

[a] The different critical ice nucleation parameters, $X^*$, can be calculated from $X^* = \sum_{i=0}^{3} A_i (\ln P_{H_2O})^i$, where $P_{H_2O}$ is the water vapor pressure [in mbar], $T^*$ is the critical temperature [in K], $a_w^*$ is the critical water activity (which is equal to the critical relative humidity), $S_{ice}^*$ is the critical ice saturation ratio, and $\Delta T^*$ is the critical supercooling [in K]. These parametrizations are valid over the water vapor pressure range $2.0 \times 10^{-1}$ to $2.4 \times 10^{-4}$ mbar. For verification, at $P_{H_2O} = 10^{-2}$ mbar the above parameters yield the following values for the different $X^*$: $T^* = 209.00$, $a_w^* = 0.8977$, $S_{ice}^* = 1.640$, and $\Delta T^* = -3.584$.

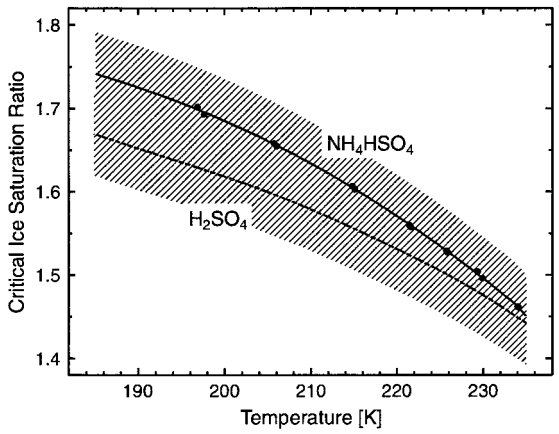


**Figure 6.** Critical ice saturation ratio for aqueous $NH_4HSO_4$ aerosols. The points are the ice saturation ratios for the experimentally determined emulsion ice freezing points (see Figure 4) as calculated with the model of Clegg et al.,[14] and the solid line is a fit to the data (for a parametrization, see Table 3). The line for $H_2SO_4/H_2O$ aerosols as given by Koop et al.[10] is also shown for comparison. The shaded area indicates the combined uncertainties of the two studies.[24]

**4.1. Thermodynamic Modeling.** The number density and size distribution of ice particles in a cloud are mainly controlled by two parameters, temperature and the critical ice saturation ratio, $S_{ice}^*$, required to nucleate ice from preexisting aerosols. $S_{ice}^*$ is defined as the ratio of the water vapor pressure of an aerosol at its freezing temperature, $T^*$, and the water vapor pressure over ice at $T^*$.

We used the model of Clegg et al.[14] to compute the critical water activity, $a_w^*$, for each droplet composition at its experimentally observed freezing temperature.[23] From these data, $S_{ice}^*$ and the cooling below the ice frost point ($\Delta T^* = T_{ice}(P^*_{H_2O}) - T^*$) were also calculated. All the parameters were fitted as a function of the water vapor pressure to allow easier comparison to field measurements. The different critical parameters for ice nucleation from aqueous $NH_4HSO_4$ aerosols are given in Table 3.

In Figure 6 we show how $S_{ice}^*$ varies as a function of temperature. The points are calculated from the experimental freezing temperatures as described above, and the solid line is the fit given in Table 3. $S_{ice}^*$ shows a steady increase with decreasing temperature ranging from 1.46 at 234 K to about 1.74 at 185 K. For comparison, $S_{ice}^*$ for aqueous sulfuric acid[10] is also shown as the dashed line in Figure 6. The values for $NH_4HSO_4$ appear to be slightly higher than the ones for $H_2SO_4$. However, the behavior of the two systems is very similar and the values agree within the estimated uncertainty of 0.05 for each study.[24]

Such high values of $S_{ice}^*$ have recently been observed in upper tropospheric wave clouds at a temperature of 209 K.[25,26] Because strong cooling due to high updraft velocities occurs in such clouds, the dominant ice particle formation mechanism in these events will most likely be homogeneous nucleation. However, field data also show lower ice saturation ratios than measured in this study.[26,27] Hence, further studies will be needed to investigate both the effect of heterogeneous nuclei[28] and also the incorporation of $HNO_3$ into ammoniated aerosols[8] on the formation of ice particles in cirrus clouds.

## 5. Conclusions

We have investigated the $NH_4HSO_4/H_2O$ phase diagram in the concentration range 0−60 wt % using differential scanning calorimetry. Phase transitions have been observed for temperatures down to 180 K. Both bulk-phase and emulsion studies agree closely with the results from the thermodynamic model of Clegg et al.[14] and indicate that ice, letovicite, and SAT are the crystalline phases present in our experiments. The melting points obtained in this study differ from the phase diagram reported by Imre et al.,[13] especially for the ice melting point curve. However, our results are in very good agreement with the recent melting point investigations by Yao et al.[15] and Chelf and Martin.[16]

Emulsified aqueous $NH_4HSO_4$ droplets have been investigated to study the homogeneous nucleation of ice from such aerosols. The results indicate that a high supercooling of up to 70 K is required before ice nucleates. A thermodynamic model has been used to apply the ice freezing data to the formation of clouds in the upper troposphere and lower stratosphere. The results indicate that the homogeneous nucleation of ice from $NH_4HSO_4$ aerosols in cirrus clouds requires saturation ratios with respect to ice of up to 1.7.

**Acknowledgment.** We thank S. Clegg for providing us with a code for his thermodynamic model and a preprint of their work and S. Martin for sending us a preprint of their work and providing helpful comments on the manuscript. This work was supported by grants from NASA's Atmospheric Effects of Aviation Program and the National Science Foundation. T.K. acknowledges a Feodor Lynen Fellowship from the Humboldt Foundation and an Otto Hahn Fellowship from the Max Planck Society. A.K.B. acknowledges a Natural Science and Engineering Research Council of Canada Postdoctoral Fellowship.

## References and Notes

(1) Liou, K. N. *Mon. Weather Rev.* **1986**, *114*, 1167.
(2) *Intergovernmental Panel on Climate Change (IPCC), Climate Change 1995*; Houghton, J. T., Meira Filho, L. G., Callander, B. A., Harris, N., Kattenberg, A., Marshall, K., Eds.; Cambridge University Press: Cambridge, 1996.
(3) Seinfeld, J. H. *Nature* **1998**, *391*, 837.
(4) Toon, O. B.; Miake-Lye, R. C. *Geophys. Res. Lett.* **1998**, *25*, 1109.
(5) Sheridan, P. J.; Brock, C. A.; Wilson, J. C. *Geophys. Res. Lett.* **1994**, *21*, 2587.
(6) Talbot, R. W.; Dibb, J. E.; Loomis, M. B. *Geophys. Res. Lett.* **1998**, *25*, 1367.

(7) Martin, S. T. *Geophys. Res. Lett.* **1998**, *25*, 1657.
(8) Tabazadeh, A.; Toon, O. B. *Geophys. Res. Lett.* **1998**, *25*, 1379.
(9) Bertram, A. K.; Patterson, D. D.; Sloan, J. J. *J. Phys. Chem*. **1996**, *100*, 2376.
(10) Koop, T.; Ng, H. P.; Molina, L. T.; Molina, M. J. *J. Phys. Chem. A* **1998**, *102*, 8924.
(11) Chang, H. Y. A.; Koop, T.; Molina, L. T.; Molina, M. J. *J. Phys. Chem. A* **1999**, *103*, 2673.
(12) Cziczo, D. J.; Abbatt, J. P. D. *J. Geophys. Res.* **1999**, *104*, 13781.
(13) Imre, D. G.; Xu, J.; Tang, I. N.; McGraw, R. *J. Phys. Chem. A* **1997**, *101*, 4191.
(14) Clegg, S. L.; Brimblecombe, P.; Wexler, A. S. *J. Phys. Chem. A* **1998**, *102*, 2137.
(15) Yao, Y.; Massucci, M.; Clegg, S. L.; Brimblecombe, P. *J. Phys. Chem. A* **1999**, *103*, 3678.
(16) Chelf, J. H.; Martin, S. T. *Geophys. Res. Lett.* **1999**, *26*, 2391.
(17) Schäfer, K., Lax, E., Eds. *Landoldt-Börnstein, Zahlenwerte und Funktionen*; Springer: Berlin, 1962; Part 2, Vol. b.
(18) Molina, M. J.; Zhang, R.; Wooldridge, P. J.; McMahon, J. R.; Kim, J. E.; Chang, H. Y.; Beyer, K. D. *Science* **1993**, *261*, 1418.
(19) Koop, T.; Biermann, U. M.; Raber, W.; Luo, B. P.; Crutzen, P. J.; Peter, T. *Geophys. Res. Lett.* **1995**, *22*, 917.
(20) Koop, T.; Luo, B. P.; Biermann, U. M.; Crutzen, P. J.; Peter, Th. *J. Phys. Chem. A* **1997**, *101*, 1117.
(21) A sample with the eutectic composition melts completely at the eutectic temperature, while a sample with a different composition melts over a range of temperatures. As a result, the largest release of latent heat at the eutectic temperature is when the sample has the eutectic composition.
(22) Pruppacher, H. R.; Klett, J. D. *Microphysics of Clouds and Precipitation*, 2nd ed.; Kluwer: Dordrecht, 1997.
(23) The 34.7 wt % emulsion samples froze at a temperature of $T^* = 178.9$ K. This is about 1 K below the lower limit of the Clegg et al. model, which is 180 K. Thus, we calculated $a_w^*$, $S_{ice}^*$, and $\Delta T^*$ for these two points by setting $T^*$ to 180 K. The corresponding error in $a_w^*$, $S_{ice}^*$, and $\Delta T^*$ is estimated to be less than 0.5% by comparing the values calculated with the model at $T^* = 180$ K and $T^* = 181$ K.
(24) For pure water the uncertainty in the droplet diameter of $1-10\ \mu$m leads to an uncertainty in $S_{ice}^*$ of about 0.03 because of the shift in freezing temperature with droplet size (see section 3.2.2.). The uncertainty in determining the freezing temperature is about $\pm 1.5$ K, yielding an additional uncertainty in $S_{ice}^*$ of 0.02.
(25) Jensen, E. J.; Toon, O. B.; Tabazadeh, A.; Sachse, G. W.; Anderson, B. E.; Chan, K. R.; Twohy, C. W.; Gandrud, B.; Aulenbach, S. M.; Heymsfield, A.; Hallett, J.; Gary, B. *Geophys. Res. Lett.* **1998**, *25*, 1363.
(26) Heymsfield, A. J.; Miloshevich, L. M.; Twohy, C.; Sachse, G.; Oltmans, S. *Geophys. Res. Lett.* **1998**, *25*, 1343.
(27) Heymsfield, A. J.; Miloshevich, L. M. *J. Atmos. Sci.* **1995**, *52*, 4302.
(28) DeMott, P. J.; Rogers, D. C.; Kreidenweis, S. M.; Chen, Y. L.; Twohy, C. H.; Baumgardner, D.; Heymsfield, A. J.; Chan, K. R. *Geophys. Res. Lett.* **1998**, *25*, 1387.